International Research Journal of Multidisciplinary Scope (IRJMS), 2024; 5(3):751-759

Original Article | ISSN (O): 2582-631X DOI: 10.47857/irjms.2024.v05i03.0969

# Robust Remote Sensing Image Classification utilizing Multiverse Optimization Model with Deep Transfer Learning Approach

Josephine Anitha A[1]*, Gladis D[2]

[1]Department of Computer Science, Presidency College (Autonomous), University of Madras, Chennai-600005, India, [2]Bharathi Women's College, Chennai-600108, India. *Corresponding Author's Email: anitharesearchscholar@gmail.com

## Abstract

The classifying process of Remote Sensing Image (RSI) has been crucial in diverse applications, involving land cover mapping, environmental monitoring, disaster assessment, and urban planning. Conventionally, image classification in Remote Sensing (RS) relies on Machine Learning (ML) and handcrafted feature extraction approaches. But, lately, Deep Learning (DL) has become an effective and powerful method for RSI classification. DL algorithms, especially Convolutional Neural Network (CNN), have shown great performance in different Computer Vision (CV) tasks, involving image classification. This study proposes a Robust RSI Classification using Multiverse Optimization Algorithm with Deep Transfer Learning (RRSIC-MVO) model. The RRSIC-MVO technique exploits the DL with hyper-parameter selection mechanism to classify the RSI. In the presented RRSIC-MVO technique, the noise occurrence can be handled by joint bilateral filter (JBF). Following, MobileNetv3 model is applied for feature extractor and its hyper-parameters can be elected by the use of FA. Finally, soft-margin support vector machine (SM-SVM) model is applied for classification purposes. A series of investigations are accomplished on RS dataset for assessing the RRSIC-MVO model. The outputs demonstrate the effectiveness of RRSIC-MVO technique, outperforming traditional machine learning methods.

**Keywords:** Classification, Computer Vision, Deep Learning, Multiverse Optimization Algorithm, Remote Sensing Images.

## Introduction

RS plays a significant part in providing an abundance of information for various applications in the study by Lv and Liu (1). RS images (RSI) with high spectral, spatial and, temporal resolutions over wide geographical regions give a sufficient basis for the acquisition of land cover information. With the development of classification approaches, RS technique has become an effective method to attain land use information form Lv Zhang *et al*., (2). As more land cover information has been made, it has become essential to make sure the availability and accuracy of land classification products via Ma *et al*., (3). Due to its superior performance compared with that of conventional learning methods from Alkhelaiwi *et al.,* (4), Deep Learning (DL) becomes a fast developing tendency in big data analysis and extensively and effectively used in different domains, like speech enhancement, image classification in Byju *et al*., (5), Natural Language Processing (NLP) in recent times from Liang *et al.,* (6). DL architecture is represented as Artificial Neural Networks (ANNs), including commonly two or more layers. Deep Neural Network (DNN) utilizes feature representations learned entirely from information from Tong *et al.,* (7). But they do not need handcrafted features that are commonly developed based on the domain-specific knowledge. This prevents the issue that handcrafted feature was dependent heavily on domain knowledge Pu *et al.,* (8). Moreover, it is not practical to meet the requirement of the data embedded in any form by using predetermined handcrafted features by Xu *et al*., (9). DL technique is capable of automatically learning useful representation of raw input dataset with various levels of abstraction rather than relying on shallow manually engineered feature Li *et al.,* (10).

This study proposes a Robust RSI Classification using Multiverse Optimization Algorithm with Deep Transfer Learning (RRSIC-MVO) model. The RRSIC-MVO technique exploits the DL with hyper-parameter selection mechanism to classify the RSI. In the presented RRSIC-MVO technique, the noise



(Received 19th April 2024; Accepted 19th July 2024; Published 30th July 2024)

occurrence can be handled by joint bilateral filter (JBF). Following, MobileNetv3 model is applied for feature extractor and its hyper-parameters can be elected by the use of FA. Finally, Soft-Margin Support Vector Machine (SM-SVM) method is applied for classification purposes. A series of investigations are accomplished on RS dataset to assess the RRSIC-MVO method. In the study, Ma *et al*., (11), a collective Neural Network (NN) system known as the Fuzzy Deep Learning Conditional Random Field Network (FCUnet) is presented for solving the advanced segmenting of HRRS. Firstly, a fuzzy U-Net classification networking is constructed for attaining efficient feature data that presents the Fuzzy Logic Unit (FLU) into the networking for processing the HRRS' uncertainty and ambiguity. Later, the authors present the Conditional Random Field (CRF) after FCUnet for optimizing the outcomes of the image segmenting process. In the existing work, Firat *et al*., (12), a fusion 3D Residual Spatial–Spectral Convolution Network (3D-RSSCN) is presented for extracting Deep Spatio-Spectral aspects by implementing ResNet18 and 3D CNN construction. Concurrently, feature extracting process of Spatio-Spectral is given by employing 3D CNN. In the deep CNNs, ResNet construction is implemented for achieving greater classifying accomplishment as the layer numbers rise. Additionally, due to the ResNet construction, issues like vanishing gradient and degradation that may happen in deep networks are surmounted. In the present research, PCA is employed as pre-processing technique for optimal spectral band extracting process.

Chebbi *et al.,* (13) proposes a model for storing a tremendous number of diverse satellite imageries based on Apache Spark and Hadoop Distributed File System (HDFS) methods. Deep Learning (DL) methods like UNet and VGGNet are also introduced which can be useful for the processing of huge RS data to classify and extract the factors. Joshi *et al.,* (14) introduce an Ensemble Of DL-Based Multimodal Land Cover Classification (EDL-MMLCC) methods by employing RSI. Initially, Median Filtering (MF) based data augmenting and pre-processing models happen. Additionally, a collection of DL approaches, called MobileNet, VGG-19, and Capsule Network (CapsNet), are implemented for the feature extracting process. Also, the DL method's training procedure was improved by the utilization of Hosted Cuckoo Optimization (HCO) model. Lastly, the Regularized Extreme Learning Machine (RELM) with Salp Swarm Algorithm (SSA) classifier is enforced for classifying the land cover data.

Li *et al.,* (15) introduce an Adaptive Multiscale Deep Fusion ResNet (AMDF-ResNet) model. The presented model comprises two networks (i) backbone and (ii) fusion. The first network comprising various residual blocks produces multi-scale ranking factors that consist of semantic data from lower to higher levels. Next, the presented AMDF module can accentuate beneficial data and suppresses unnecessary data by learning the weight that depicts the significance of the feature. In the existing study, Ye *et al.*, (16), an RSI classification model based on the integration of the SVM and DL feature techniques is presented. Initially, as the behaviour of the DL method requires tremendous training information, the clipping and rotation for enhancing the original RSI numbers are operated. Later, the enhanced information is segmented into the two-fold testing, training, and validation sets. The CNN parameters are put under training by the validation and training set, and the initial testing sample features are extracted on the basis of the trained CNN approach.

# Methodology

This paper has developed an automated RRSIC-MVO model. The RRSIC-MVO technique exploits the DL with hyperparameter selection mechanism to classify the RS images. It includes four processes such as JBF, MobileNetv3, MVO based tuning, and SM-SVM classifier. Figure 1 describes the entire flow of RRSIC-MVO approach.

## Stage I: JBF Pre-processing

The JBF method considerably contributes to retaining the edge details existing in the images from Alarmgir and Alam (17). Based on the intensity of the images, the typical BF maintains the edge data. However, this filter will not be able to preserve the edge image data with low intensity. Thus, the proposed method exploits the JBF filtering method to resolve these drawbacks. The initial major element is utilized as a guiding image substituting the kernel filtering range for preserving the edge data more effectively than the conventional filter.

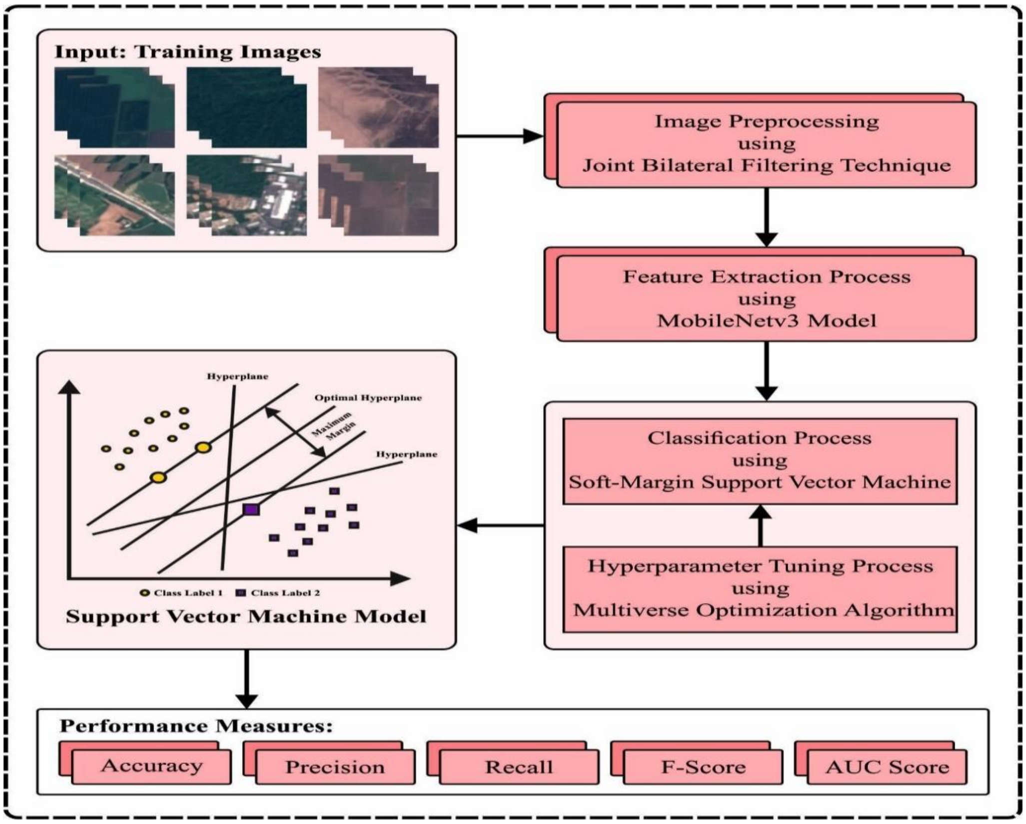


**Figure 1:** Overall Flow of RRSIC-MVO Algorithm

## Stage II: Optimal MobileNetv3

For feature extractor, the MobileNetv3 model is used. MobileNetV3 is a family of effective NN structures developed for embedded and mobile devices with limited computation resources from Yang and Han (18). The objective is to enhance efficiency of the model while preserving higher accuracy in CV tasks including object detection and image classification. It accomplishes this by integrating design choices and architectural advancements: It presents a new search space that enables automated neural architecture search (NAS) to search the optimum structure. This technique allows the discovery of efficient and compact model configurations personalized for certain tasks or target platforms.

In this work, the hyper-parameters can be elected by the use of MVO algorithm Fang *et al*., (19). The MVO technique includes comparatively low performance parameters, mainly including the wormhole travel distance rate and wormhole existence probability. Generally, the low dimensional mathematical experiment delivers comparatively good performances. Like other SI optimization techniques, the optimization technique of the MVO technique can be split into two phases: development and exploration. Black and White holes are utilized for exploration, while Wormholes are exploited for the development. The MVO technique follows the subsequent rules as follows:

- A high inflation rate of universe improves the chances of considerable amount of white holes.
- In contrast, when the inflation rate of universe is comparatively lower, then the black holes are highly possibly made.
- The universe that formed white holes resist the object.
- On the contrary, the universe that formed black holes absorbs the object.
- Despite the inflation rate, other universes transmit objects towards the present optimum universe via wormholes.

Based on the principles of wormholes and white or black holes, the MVO technique generates the initial universe iterative loop. Especially, the fitness value of solution shows the inflation rate of universe, the universe refers to the potential solution to the problems, and the object in the universe refers to the component of the solution. The mathematical expression can be described as follows:

$$U = [x_1^1\ x_1^2\ \dots\ x_1^d\ x_2^1\ x_2^2\ \dots\ x_2^d\ \vdots\vdots\vdots\vdots\ x_n^1\ x_n^2\ \dots\ x_n^d\ ] \qquad [1]$$

In Eq. [1], $n$ shows the amount of candidate solutions (universes) and $d$ indicates the amount of variables (objects).

Meanwhile, all the universes manifest the single inflation rate, the object in the universe migrated via the orbits of black or white holes. The roulette wheel mechanism can be given in the following:

$$x_i^j = \{x_k^j \, r_1 < NI(Ui) \;\; x_i^j \;\; r_1 \geq NI(Ui)\,' \qquad [2]$$

In Eq. [2], $U_i$ shows the $i^{th}$universes, $x_i^j$ indicates the location of the $j^{th}$ object black holes in the $i^{th}$ universes, $x_k^j$ shows the location of the $j^{th}$ objects of the $k^{th}$ universes produced by the roulette mechanism and $NI\ (Ui)$ shows the infation rate of $i^{th}$ medium universes.

Irrespective of the inflation rate, the local variation is accomplished and increased if the universe object stimulates the internal object for travelling towards the present optimum universe. $H$ denotes the threshold, and take the empirical values as $H = 0.5$; $r_2$, $r_3$, and $r_4$ indicates an arbitrary value in [0,1]; $lb$ and $ub$ shows the lower and upper variable limitations; $Bestx_i^j$ shows the location of wormhole respective to the present optimum universe. Then, the optimum position is continually updated. Once $x_{i+1}^j$, an optimum universe wormhole position is created, then the universe inflation rate between $x_{i+1}^j$and $x_i^j$ would be compared. When the fitness values of $x_{i+1}^j$ is greater than $x_i^j$, $x_{i+1}^j$ replaces $x_i^j$; or else, $x_i^j$ is retained for the following generation.

The mathematical model of $WEP$ is given below:

$$WEP = WEP\frac{l}{L}(WEPmin_{max})_{min} \qquad [3]$$

In Eq. [3], $WEP_{max}$ and $WEP_{min}$ denotes the empirical value $WEP_{max} = 1$ and $WEP_{min} = 0.2$, correspondingly, $l$ specifies the present amount of iterations, and $L$ shows the maximal amount of iterations. Furthermore, the TDR was formulated by Eq. [4]:

$$TDR = 1 - \left(\frac{l}{L}\right)^{\frac{1}{p}} \qquad [4]$$

Here, $p$ shows the accuracy of the mining capacity. The process of selecting a fitness function (FF) is a significant aspect in the MVO technique. Solution encoding is employed to measure the solution candidate goodness. The accuracy output is the initial condition employed in designing a FF.

$$Fitness = max\ (P) \qquad [5]$$

$$P = \frac{TP}{TP + FP} \qquad [6]$$

Where $TP$ and $FP$ characterize the true and false positive values.

## Stage III: Image Classification

The SM-SVM model is applied for classifying the imaging into diverse classes. The proposed method is utilized for image classification from Liang *et al.,* (20). It extends the Maximal Separating Margin SVM (hard margin SVM) Helber *et al.,* and Bonet *et al.*, (21, 22) therefore, the hyperplane permits the existence of noisy information. Here, $\xi_i$, a Slack factor is used to consider the violation of the classification model anlysis from Naushad *et al.*, (23).

$$Wx_i + b \geq 1 - \xi_i, \forall y_i = +1, \qquad [7]$$
$$Wx_i + b \leq -1 + \xi_i, \forall y_i = -1;$$

Thus,

$$y_i(Wx_i + b) \geq 1 - \xi_i, i = 1,2,\dots,n. \qquad [8]$$

The Primal issue can be represented as follows.

$$\frac{1}{2}\|W\|^2 + C\sum_{i=1}^{n} \xi_i \qquad [9]$$
$$s.t.\ y_i(Wx_i + b) \geq 1 - \xi_i,$$
$$\xi_i \geq 0, i = 1,2,\dots,n.$$

The Dual Problem Function of SM is given below.

$$W(\alpha) = \sum_{i=1}^{n} \alpha_i - \frac{1}{2}\sum_{i=1j}^{n} \sum_{=1}^{n} \alpha_i\alpha_j y_i y_j x_i^T x_j$$
$$s.t. \sum_{i=1}^{n} \alpha_i y_i = 0 \qquad [10]$$
$$0 \leq \alpha_i \leq C, i = 1,2,\dots,n.$$

KKT complementary condition in inseparable instance can be formulated below.

$$\alpha_i[y_i(Wx_i + b) - 1 + \xi_i] = 0, i = 1,2,\dots,n, \qquad [11]$$
$$\beta_i\xi_i = 0, i = 1,2,\dots,n, \qquad [12]$$

where $\beta_i$ indicates Lagrange Multipliers corresponding to $\xi_i$ that was presented to enforce non-negativity of $\xi_i$.

$$\alpha_i + \beta_i = C \qquad [13]$$

With the consideration of Eqs. (12) and (13), Eq. (14) can be designed.

$$\xi_i = 0\ if \alpha_i < C. \qquad [14]$$

Consequently, optimal weight $W^*$ can be derived using Eq. (15).

$$W^* = \sum_{i=1}^{n} \alpha_i^* y_i x_i. \quad [15]$$

The optimum bias $b^*$ can be obtained by samples $(x_i, y_i)$ in the train data where $0 < \alpha_i^* < C$ and $\xi_i = 0$, as given below.

$$b^* = 1 - \xi_i - \sum_{sv} \alpha_i^* y_i x_i x_s, \qquad \forall y_s = +1. \quad [16]$$

## Results and Discussion

The classification outputs of the RRSIC-MVO system are investigated on the EUROSAT dataset Helber *et al.,* (21), and the dataset description is depicted in Table 1. Figure 2 represents the instance imaging.

Figure 3 illustrates the classifier analysis of the RRSIC-MVO method under testing dataset. Figures. 3a-3b illustrates the confusion matrix provided by the RRSIC-MVO method on 70:30 of TR/TS set. The figure portrayed that the RRSIC-MVO approach has precisely detected and classified the overall 10 classes. Likewise, Figure 3c shows the curves of PR of the RRSIC-MVO approach. The figures described that the RRSIC-MVO method has reached greater PR accomplishment under 10 classes. Finally, Figure 3d illustrates the ROC value of the RRSIC-MVO method. The figure illustrated that the RRSIC-MVO method has resulted in greater outputs with higher ROC value under 10 classes.

**Table 1:** Description of Databases

| Labels | Class | Sample Numbers |
|---|---|---|
| C-1 | Annual Crop | 2000 |
| C-2 | Forest | 2000 |
| C-3 | Herbaceous Vegetation | 2000 |
| C-4 | Highway | 2000 |
| C-5 | Industrial | 2000 |
| C-6 | Pasture | 2000 |
| C-7 | Permanent Crop | 2000 |
| C-8 | Residential | 2000 |
| C-9 | River | 2000 |
| C-10 | Sea Lake | 2000 |
| **Overall Sample Numbers** | | **20000** |

**Figure 2:** Sample Images

The RSI classifier output of RRSIC-MVO METHOD on 70:30 TR/TS SET is depicted in Table 2 and Figure 4. The outputs portray the efficient detection of the RRSIC-MVO approach on distinct classes. On 70% of TR set, the RRSIC-MVO approach presents an average $accu_y$ of 95.86%, $prec_n$ of 79.26%, $reca_l$ of 79.28%, $F_{score}$ of 79.21%, and $AUC_{score}$ of 88.49%. Also, on 30% of TS set, the RRSIC-MVO approach presents an average $accu_y$ of 95.82%, $prec_n$ of 79.07%, $reca_l$ of 79.09%, $F_{score}$ of 79.02%, and $AUC_{score}$ of 88.38%.

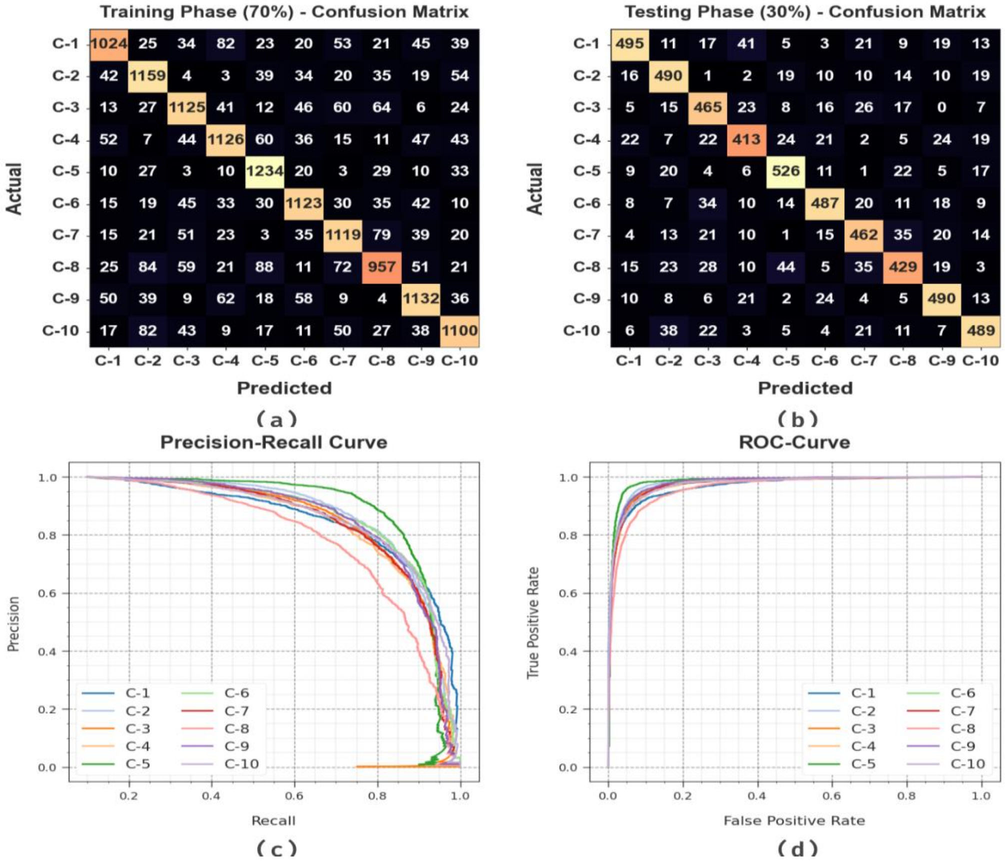


**Figure 3:** Performance of (a-b) 70: 30 TR/TS set, (c-d) Curves of PR and ROC

**Table 2:** RSI Classifier Output of RRSIC-MVO Method on 70:30 TR/TS Set

| Class | $Accu_y$ | $Prec_n$ | $Reca_l$ | $F_{score}$ | $AUC_{score}$ |
|---|---|---|---|---|---|
| **Training Phase (70%)** | | | | | |
| Annual Crop (C-1) | 95.85 | 81.08 | 74.96 | 77.90 | 86.54 |
| Forest (C-2) | 95.85 | 77.79 | 82.26 | 79.96 | 89.81 |
| Herbaceous Vegetation (C-3) | 95.82 | 79.39 | 79.34 | 79.37 | 88.51 |
| Highway (C-4) | 95.72 | 79.86 | 78.14 | 78.99 | 87.94 |
| Industrial (C-5) | 96.89 | 80.97 | 89.49 | 85.02 | 93.59 |
| Pasture (C-6) | 96.21 | 80.56 | 81.26 | 80.91 | 89.56 |
| Permanent Crop (C-7) | 95.73 | 78.20 | 79.64 | 78.91 | 88.58 |
| Residential (C-8) | 94.74 | 75.83 | 68.90 | 72.20 | 83.24 |
| River (C-9) | 95.84 | 79.22 | 79.89 | 79.55 | 88.76 |
| SeaLake (C-10) | 95.90 | 79.71 | 78.91 | 79.31 | 88.34 |
| **Average** | **95.86** | **79.26** | **79.28** | **79.21** | **88.49** |
| **Testing Phase (30%)** | | | | | |
| Annual Crop (C-1) | 96.10 | 83.90 | 78.08 | 80.88 | 88.15 |
| Forest (C-2) | 95.95 | 77.53 | 82.91 | 80.13 | 90.14 |
| Herbaceous Vegetation (C-3) | 95.47 | 75.00 | 79.90 | 77.37 | 88.52 |
| Highway (C-4) | 95.47 | 76.62 | 73.88 | 75.23 | 85.78 |

| | | | | | |
|---|---|---|---|---|---|
| Industrial (C-5) | 96.38 | 81.17 | 84.70 | 82.90 | 91.22 |
| Pasture (C-6) | 96.00 | 81.71 | 78.80 | 80.23 | 88.39 |
| Permanent Crop (C-7) | 95.45 | 76.74 | 77.65 | 77.19 | 87.53 |
| Residential (C-8) | 94.82 | 76.88 | 70.21 | 73.40 | 83.91 |
| River (C-9) | 96.42 | 80.07 | 84.05 | 82.01 | 90.90 |
| Sea Lake (C-10) | 96.15 | 81.09 | 80.69 | 80.89 | 89.29 |
| **Average** | **95.82** | **79.07** | **79.09** | **79.02** | **88.38** |

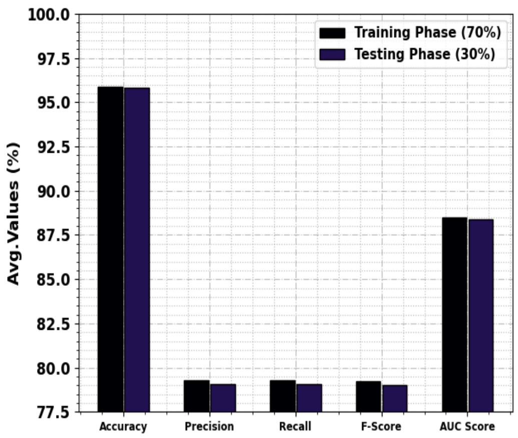


**Figure 4:** Average Output of RRSIC-MVO System on 70:30 TR/TS Set


**Figure 5:** $Accu_y$ Curve of the RRSIC-MVO System

Figure 5 portrayed the $TR\_accu_y$ and $VL\_accu_y$ of the RRSIC-MVO method. The $TL\_accu_y$ is defined by assessing the RRSIC-MVO method on TR dataset, while the $VL\_accu_y$ is calculated by assessing the achievement on a discrete test dataset. The outputs exhibited that $TR\_accu_y$ and $VL\_accu_y$ surges with an epoch growth. Hence, the achievement of the RRSIC-MVO approach obtains greater TR/TS dataset with maximum epoch count. Figure 6 portrayed the $TR\_loss$ and $VR\_loss$ of the RRSIC-MVO method. The $TR\_loss$ portrays the error amid the anticipated and initial TR dataset. The $VR\_loss$ portrayed the accomplishment measure of the RRSIC-MVO method on a distinct validation data. The outputs denoted that the loss values lessen as epoch surges. It portrayed the enhanced achievement of the RRSIC-MVO approach and its capacity in producing a precise classification. The lessened loss values portrayed the greater achievement of the RRSIC-MVO approach in comprehending the relationships and patterns.

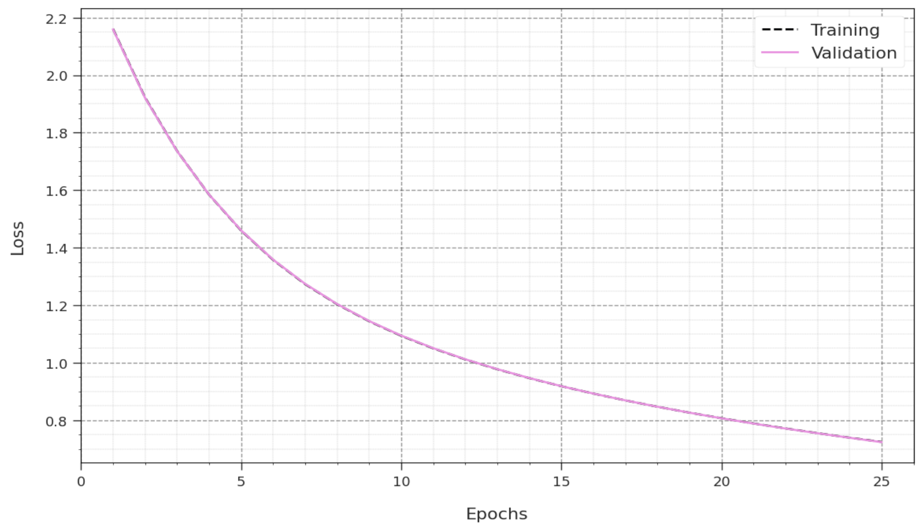


**Figure 6:** Loss Curve of the RRSIC-MVO System

**Table 3:** $Accu_y$ Output of RRSIC-MVO Approach with Recent Methodologies

| Model | Accuracy (%) |
|---|---|
| RF | 61.46 |
| VGG16 | 94.15 |
| CNN | 94.09 |
| ResNet-50 | 94.25 |
| SimCLR | 92.59 |
| MoCo-v2 | 93.78 |
| BYOL | 94.02 |
| RRSIC-MVO | 95.86 |

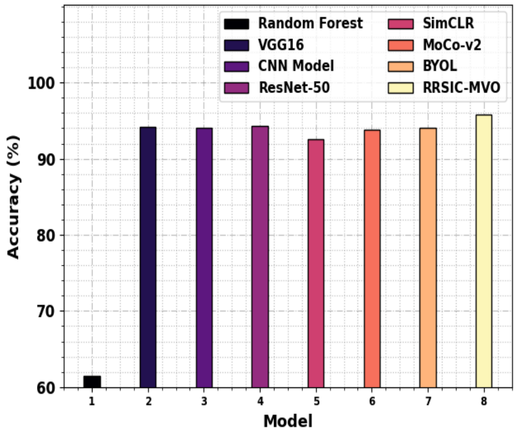


**Figure 7:** $Accu_y$ Outcome of RRSIC-MVO System with Recent Methods

In Table 3 and Figure 7, a series of analysis were achieved to assure the significant achievement of the RRSIC-MVO approach. The results illustrated that the RRSIC-MVO approach reaches greater $accu_y$ of 95.86%. At the same time, the RF, VGG16, CNN, ResNet-50, SimCLR, MoCo-v2, and BYOL techniques have resulted in a lessened $accu_y$ of 61.46%, 94.15%, 94.09%, 94.25%, 92.59%, 93.78%, 94.02%, and 95.86% subsequently. Thus, the RRSIC-MVO technique can be employed for automated RS image classification.

## Conclusion

This paper has developed an automated RRSIC-MVO algorithm. The RRSIC-MVO technique exploits the DL with hyper-parameter selection mechanism to classify the RSI. In the presented RRSIC-MVO technique, the noise occurrence can be handled by the JBF. Following, MobileNetv3 model is applied for feature extractor and its hyper-parameters can be elected by the use of MVO algorithm. Finally, the SM-SVM model is applied for classification purposes. A sequence of investigations is carried out on RS datasets to evaluate the RRSIC-MVO model. The outcome illustrates the effectiveness of RRSIC-MVO technique, outperforming traditional machine learning methods. In the future, hybrid metaheuristic hyper-parameter optimizer can be developed to improve the results of the RRSIC-MVO model.

## Abbreviations

Nil.


## Acknowledgement

Nil.


## Author contributions

All Authors contributed equally.

## Conflict of Interest

The authors have expressed no conflict of interest.

## Ethics Approval

Not applicable.


## Funding

The authors did not receive support from any organization for the submitted work.


## References


1. Lv Z, Liu T, Benediktsson JA. Object-oriented key point vector distance for binary land cover change detection using VHR remote sensing images. IEEE Transactions on Geoscience and Remote Sensing. 2020 Mar 13;58(9):6524-33.
2. Lv Q, Zhang S, & Wang Y. Deep learning model of image classification using machine learning. Advances in Multimedia, 2022(1), 3351256.
3. Ma H, Liu Y, Ren Y, Wang D, Yu L, Yu J. Improved CNN classification method for groups of buildings damaged by earthquake, based on high resolution remote sensing images. Remote Sensing. 2020 Jan 11;12(2):260.
4. Alkhelaiwi M, Boulila W, Ahmad J, Koubaa A, Driss M. An efficient approach based on privacy-preserving deep learning for satellite image classification. Remote Sensing. 2021 Jun 6;13(11):2221.
5. Byju AP, Sumbul G, Demir B, Bruzzone L. Remote-sensing image scene classification with deep neural networks in JPEG 2000 compressed domain. IEEE Transactions on Geoscience and Remote Sensing. 2020 Jul 20;59(4):3458-72.
6. Liang P, Shi W, Zhang X. Remote sensing image classification based on stacked denoising autoencoder. Remote Sensing. 2017 Dec 22;10(1):16.
7. Tong XY, Xia GS, Lu Q, Shen H, Li S, You S, Zhang L. Land-cover classification with high-resolution remote sensing images using transferable deep models. Remote Sensing of Environment. 2020 Feb 1;237:111322.
8. Pu S, Wu Y, Sun X, Sun X. Hyperspectral image classification with localized graph convolutional filtering. Remote Sensing. 2021 Feb 2;13(3):526.

9. Xu Z, Liu G, Xiao G, Tang L, Li Y. JCa2Co: A joint cascade convolution coding network based on fuzzy regional characteristics for infrared and visible image fusion. IET Computer Vision. 2021 Oct;15(7):487-500.
10. Li Y, Zhang H, Xue X, Jiang Y, Shen Q. Deep learning for remote sensing image classification: A survey. Wiley Interdisciplinary Reviews: Data Mining and Knowledge Discovery. 2018 Nov;8(6):e1264.
11. Ma X, Xu J, Chong Q, Ou S, Xing H, Ni M. FCUnet: Refined remote sensing image segmentation method based on a fuzzy deep learning conditional random field network. IET Image Processing. 2023 Oct;17(12):3616-29.
12. Firat H, Asker ME, Bayindir MI, Hanbay D. 3D residual spatial–spectral convolution network for hyperspectral remote sensing image classification. Neural Computing and Applications. 2023 Feb;35(6):4479-97.
13. Chebbi I, Mellouli N, Farah IR, Lamolle M. Big remote sensing image classification based on deep learning extraction features and distributed spark frameworks. Big Data and Cognitive Computing. 2021 May 5;5(2):21.
14. Joshi GP, Alenezi F, Thirumoorthy G, Dutta AK, You J. Ensemble of deep learning-based multimodal remote sensing image classification model on unmanned aerial vehicle networks. Mathematics. 2021 Nov 22;9(22):2984.
15. Li G, Li L, Zhu H, Liu X, Jiao L. Adaptive multiscale deep fusion residual network for remote sensing image classification. IEEE Transactions on Geoscience and Remote Sensing. 2019 Jun 26;57(11):8506-21.
16. Ye Q, Xu D, Zhang D. Remote sensing image classification based on deep learning features and support vector machine. Journal of Forestry Engineering. 2019;4(2):119-25.
17. Alamgir FM, Alam MS. An artificial intelligence driven facial emotion recognition system using hybrid deep belief rain optimization. Multimedia Tools and Applications. 2023 Jan;82(2):2437-64.
18. Yang Y, Han J. Real-Time object detector based MobileNetV3 for UAV applications. Multimedia Tools and Applications. 2023 May;82(12):18709-25.
19. Fang JC, Zeng AF, Zheng SF, Zhao WD, He X. Improved Multiverse Optimization Algorithm for Fuzzy Flexible Job-Shop Scheduling Problem. IEEE Access. 2023 May 16;11:48259-75.
20. Liang H, Bai H, Liu N, Sui X. Polarized skylight compass based on a soft-margin support vector machine working in cloudy conditions. Applied Optics. 2020 Feb 10;59(5):1271-9.
21. Helber P, Bischke B, Dengel A, Borth D. Eurosat: A novel dataset and deep learning benchmark for land use and land cover classification. IEEE Journal of Selected Topics in Applied Earth Observations and Remote Sensing. 2019 Jun 14;12(7):2217-26.
22. Bonet C, Chapel L, Drumetz L, Courty N. Hyperbolic sliced-wasserstein via geodesic and horospherical projections. InTopological, Algebraic and Geometric Learning Workshops 2023 2023 Sep 27 (pp. 334-370). PMLR.
23. Naushad R, Kaur T, Ghaderpour E. Deep transfer learning for land use and land cover classification: A comparative study. Sensors. 2021 Dec 3;21(23):8083.